

# Observed and simulated sea breeze characteristics over Rayong coastal area, Thailand

Tung Thanh Phan · Kasemsan Manomaiphiboon

Received: 13 January 2011 / Accepted: 14 March 2012 / Published online: 11 April 2012  
© Springer-Verlag 2012

**Abstract** This work presents the detailed characterization of sea breeze (SB) over the Rayong coastal area, one of the most rapidly developed and highly industrialized areas during the last decade in Thailand, using observation data analysis and fine-resolution (2 km) mesoscale meteorological modeling with incorporation of new land cover and satellite-derived vegetation fraction data sets. The key characteristics considered include frequency of SB occurrence, sea-breeze day (SBD) identification, degree of inland penetration, and boundary layer development. It was found that SBs occur frequently in the winter due mainly to relatively large land–sea temperature contrasts and minimally in the wet season. Monthly mean SB onset and cessation times are at around 12–15 local time (LT) and 18–21 LT, respectively, and its strength peaks during the early- to mid-afternoon. Monthly SB hodographs generally exhibit clockwise rotations, and SB inland penetration (at PCD-T tower) ranges widely with the monthly means of 25–55 km from the coast.

Mesoscale MM5 modeling was performed on two selected SBDs (13 January and 16 March 2006), on which the SBs are under weak and onshore strong influences from background winds, respectively. Simulated near-surface winds and temperature were found to be in fair-to-acceptable agreement with the observations. The SB circulation along the Rayong coast is clearly defined with a return flow aloft and a front on 13 January, while it is enhanced by the onshore background winds on 16 March. Another SB along the Chonburi coast also develops separately, but their fronts merge into one in the mid-afternoon, resulting in large area coverage by the SB. Simulated planetary boundary layer height over the land area is significantly affected by a thermal internal boundary layer (TIBL) induced by an SB, which is found to be low near the coast and increases toward the front (up to 800–1,000 m along the Rayong coast).

## 1 Introduction

Sea breeze (SB) is a thermally forced circulation that usually occurs along coastal areas, when a land surface becomes warmer than the adjacent sea during the daytime. Its formation is mainly driven by the differential temperature of the air surface over the land and the sea. When the SB penetrates inland, it is marked with a decrease in temperature, an increase in humidity of the atmosphere, and the formation of a thermal internal boundary layer (TIBL) (Abbs and Physick 1992; Lin et al. 2001). The evolution and characteristics of an SB are influenced by several factors such as synoptic winds, topography, and Coriolis force (Haurwitz 1947; Abbs and Physick 1992; Arritt 1992; Miao et al. 2003; Miller et al. 2003; Srinivas et al. 2006; Crosman and Horel 2010). The TIBL induced by the SB can limit the vertical extent of air pollutant

Responsible editor: J.-F. Miao.

**Electronic supplementary material** The online version of this article (doi:10.1007/s00703-012-0185-9) contains supplementary material, which is available to authorized users.

T. T. Phan · K. Manomaiphiboon (✉)  
The Joint Graduate School of Energy and Environment (JGSEE),  
King Mongkut's University of Technology Thonburi (KMUTT),  
126 Prachauthit Rd., Bangmod, Tungkru,  
Bangkok 10140, Thailand  
e-mail: kasemsan\_m@jgsee.kmutt.ac.th

T. T. Phan  
e-mail: tungpts194@gmail.com

T. T. Phan · K. Manomaiphiboon  
Center for Energy Technology and Environment,  
Ministry of Education, Bangkok, Thailand

dispersion (Srinivas et al. 2006) and may lead to a fumigation event in an area that has elevated air pollutant sources on or near its coast (Lin et al. 2001). Papanastasiou and Melas (2009) also addressed the degrees of stagnation, ventilation, and recirculation of SB-associated weather in relation to local air pollution. Thus, understanding SB characteristics and the associated boundary layer development are important for air quality management in a coastal urbanized or industrialized area. A large number of studies on the SB have been conducted over many areas around the world using observations and atmospheric modeling. Most observational and modeling studies emphasize on general SB characterization and impacts on transport and dispersion of air pollutants. Atmospheric or meteorological modeling has also aided investigating the time-dependent vertical structure of SB in both horizontal and vertical spatial scales, and on physical processes involved (e.g., Lin et al. 2001; Ding et al. 2004; Srinivas et al. 2006; Pushpadas et al. 2010). Arritt (1992) reported that prevailing onshore synoptic winds of a few meters per second (or larger) are sufficient to suppress SB development, while it is still possible for an SB to develop under strong offshore (opposing) synoptic winds (as strong as 11 m/s). The SB onset time can be significantly delayed under offshore synoptic winds, but is early under onshore synoptic winds (Azorin-Molina and Chen 2008). Topography is known to play a certain role in aligning an SB in front of the coastline, constraining convergence zones close to a mountain range (Miao et al. 2003) and controlling the degree of inland penetration (Abbs and Physick 1992).

The onshore/offshore nature of horizontal SB circulation may be examined using wind hodographs. Clockwise turnaround or rotation of the SB with time is typically seen in the Northern Hemisphere (Haurwitz 1947), though some exceptions have the opposite direction over particular locations (Kusuda and Alpert 1983; Simpson 1994; Furberg et al. 2002). The onshore/offshore nature of horizontal SB circulation may be examined using wind hodographs. Clockwise turnaround or rotation of the SB with time is typically seen in the Northern Hemisphere (Haurwitz 1947), though some exceptions have the opposite direction over particular locations (Kusuda and Alpert 1983; Simpson 1994; Furberg et al. 2002). Many studies applied the PSU/NCAR mesoscale model MM5 and found the model's capability of simulating land-sea breeze circulations well (e.g., Lin et al. 2001; Ding et al. 2004; Srinivas et al. 2006; Chen et al. 2009; Dandou et al. 2009; Lu et al. 2009; Miao et al. 2009). Chen et al. found that aerosol transported from inland cities in the Pearl River Delta region in China to the coast was by means of the land breeze and vice versa back to the inland cities through the SB. Dandou et al. and Lu et al. examined the roles of urban heat island in SB evolution and

their interaction. Physics parameterizations accounting for atmospheric boundary layer and land surface processes are known to significantly influence SB characteristics, as shown by Miao et al. (2009) in which simulated SB structure and timing were investigated over multiple locations on the Swedish west coast using different combinations of such parameterizations in MM5. Cai and Steyn (2000) simulated the SB on the Lower Fraser Valley, Canada, using the Regional Atmospheric Model System (RAMS) (Pielke et al. 1992), showing acceptable agreement with observations for winds and temperature during the daytime but inferior performance during the nighttime. Papanastasiou et al. (2010) found near-surface wind well predicted, but near-surface temperature underpredicted by the Weather Research and Forecast (WRF) model (Skamarock et al. 2005, for version 2 used therein) over a 5-day period with SB development along the east coast of central Greece during summer. In the southeast Asia region, SB investigation has been relatively limited, and some examples are Hadi et al. (2002) for the city of Jakarta in Indonesia and Joseph et al. (2008) for a selected area on the Malay Peninsula.

To the authors' knowledge, no evident or dedicated research works on this subject have been conducted for Thailand. As a first effort to do so, this study aims to investigate the presence of the SB and its characteristics over an important area, which is the Rayong coastal area located in the eastern region of the country (see its defined spatial coverage in Fig. 1b). The Rayong coastal area is of considerable importance to Thailand in many aspects. Firstly, it has been a rapidly developed area in Thailand and one of the largest industrial zones in southeast Asia. Secondly, its continuous development has brought about occasional local air pollution problems in this area, some of which were very serious (Pollution Control Department or PCD 2007; Pham et al. 2008; Thepanondh et al. 2010). In addition, this area is known to have wind energy potential for electricity generation (Manomaiphiboon et al. 2010). Improved understanding of the roles of local meteorology in the area is fundamentally needed in support of local air pollution management, coastal environment preservation, energy-related planning, etc. In this study, a number of SB characteristics over the Rayong coastal area are of interest, including frequency of SB occurrence, sea-breeze day (SBD) identification, degree of inland penetration, boundary layer development, and influence from background flows or winds. Both observed data analysis and simulations were employed to analyze those features. The study is limited to the year 2006, primarily because it is a recent year and most of the acquired observed data are limited to this period. Moreover, the weather in this year was not affected by extreme large-scale weather perturbations (e.g., El Nino/La Nina-Southern Oscillation or ENSO) (Manomaiphiboon et al. 2010).

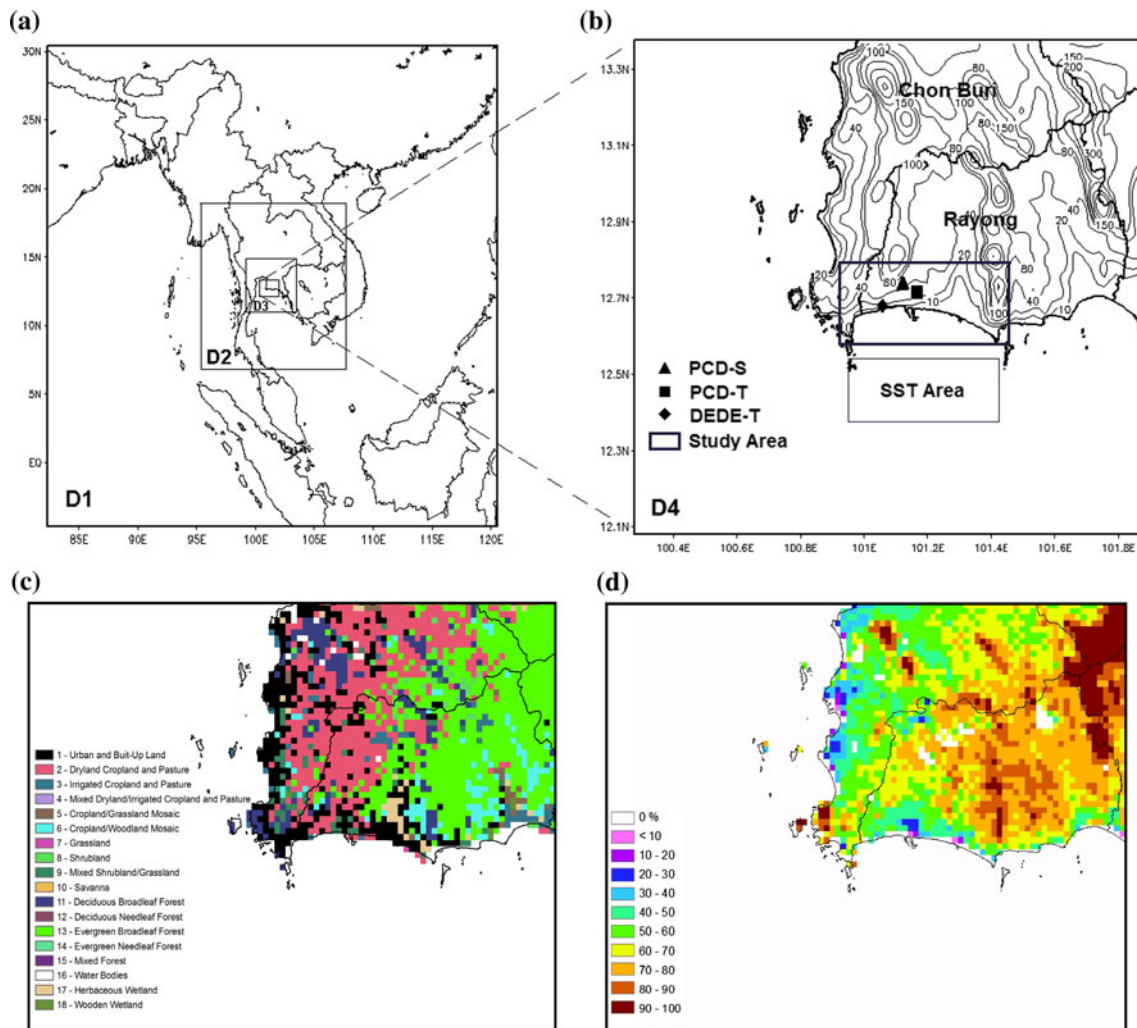


**Fig. 1** a MM5 modeling domains (D1–D4). b Terrain elevation over D4, locations of monitoring station, and SST area, c New land cover map over D4, and d new vegetation fraction (from January as example) map over D4

## 2 Methods

### 2.1 Description of study area

The Rayong coastal area is part of the Rayong Province (centered at 12.7°N lat. and 101.2°E lon.) in the eastern region (Fig. 1b). Its entire coastline (over the entire province) is about 90-km long, aligned in the east–west direction and adjacent to the Gulf of Thailand to the south. But, only its half portion to the east is considered as our focused study area (i.e., Rayong coastal area). Despite industrial and urban developments, the study area is still not deemed as a large city. Most residential buildings in the area are not tall (<5 floors, as a rough estimate). Nevertheless, there are large industrial facilities and power plants present in the area. From our field survey in 2009, the overall spatial arrangement of its built-up portion was generally aligned with the coastline and not tightly formed. There are

currently only two major highways passing through the area and no major encircling beltways are present. In comparison with the total built-up portion of the Bangkok Metropolitan, that of the Rayong coastal area is much smaller (10 times), based on LDD (2007)'s GIS data. As for the eastern region, its topography is somewhat diverse, characterized by a combination of coastal plains, valleys, hills, and short mountain ranges, while the Rayong coastal area is relatively flat with the presence of only a few small hills. Along the west side of the region is the Chonburi coast. It stretches north–south about 90 km, as part of the Chonburi Province. The general climate of the area is also compatible with that of Thailand, which is under the influence of two prevailing monsoons: the southwesterly and the northeasterly (Thai Meteorological Department or TMD 2010). The former normally starts in mid-May and ends in mid-October, bringing warm moist air from the Indian Ocean and abundant precipitation (i.e., wet season).

The latter begins in mid-November and ends in mid-February, bringing cold dry air from China (i.e., dry season or winter). The transitional period from the northeasterly to southwesterly monsoons marks the warmest period of the year (i.e., summer), and the other monsoonal transitional period is between late October and early November when the weather begins to switch from warm moist to cold dry.

## 2.2 Observed data

The availability of meteorological data routinely monitored in the area, though not considerable but still adequate, allowed this study to be technically possible. Hourly wind and air temperature data came from two sources: the PCD and the Department of Alternative Energy Development and Efficiency (DEDE), Ministry of Energy. They were collected from routine monitoring at a surface station of the PCD (to be referred to as PCD-S), at a 100-m (above the ground or AGL) tower of the PCD (to be referred to as PCD-T) and a 40-m wind tower of the DEDE (to be referred to as DEDE-T) (see their locations in Fig. 1b). The general station information is given in Table 1. Both towers are 5–6 km apart (along the north–south direction) and about 10 km apart location-wise. As seen, at PCD-T, wind (both speed and direction) was measured at 50 and 100 m, while at DEDE-T wind speed was measured at 30 and 40 m but wind direction was only measured at 40 m. The wind direction values from both measurement heights at PCD-T are not much different, with a mean difference of 16°. It is noted that a limited number of elevated monitoring towers (with wind measurements) are available over the area in question and that although near-surface (10–20 m) wind measurements are also present at these two towers and many other surface stations, they may not be adequately suitable or reliable for use due to significant blockage or disturbance from obstructions (based on our field survey).

For general SB characterization and to provide a common basis for result discussion here, near-surface winds with a reference height of 10 m were used and determined by extrapolating observed wind speed data from two elevated heights using a typical power-law wind profile

relationship  $U_2/U_1 = (Z_2/Z_1)^\alpha$ , where  $U_1$  and  $U_2$  are the wind speeds at heights (AGL)  $Z_1$  and  $Z_2$ , respectively, and  $\alpha$  is the wind shear exponent. The wind direction was determined using the data from the closest height to 10 m. From quality checking on the acquired data and after extrapolation, the data from PCD-T were statistically sufficient for monthly analysis (<10 % missing in each month). The data from DEDE-T were available only from January to July 2006 and also found to be near complete (<1 % missing in each month), and for the rest of the year, almost all data were missing and therefore not used. Near-surface air temperature, typically required in identification of SBDs, was from the 2-m measurements at PCD-T. Whenever missing, temperature data from PCD-T were substituted with those from PCD-S since the locations of both stations are near each other and the data are also highly correlated (correlation coefficient = 0.97). It is noted that the power-law profile is simple and straightforward for use, particularly when only a few wind measurements at different heights are available (which is the case here), but its formulation is not as rigorous or theoretical as that of the logarithmic wind profile. Nevertheless, to apply the logarithmic profile properly typically requires knowledge of additional parameters in calculation, e.g., atmospheric stability, roughness height (or also displacement height), and friction velocity or shear (van Ulden and Holtslag 1985).

## 2.3 Identification of sea-breeze days

The criteria applied here for SBD identification are based on the filtering criteria of Borne et al. (1998) as follows: an SBD is identified when (1) the wind is in offshore direction or calm for the majority of hours during the period from 6 h before sunrise until 2 h after sunrise; (2) the wind is in onshore direction for at least two consecutive hours during the period from 2 h after sunrise until 2 h after sunset; and (3) the difference between daily maximum air temperature over land and sea surface temperature (SST) (concisely referred hereafter to as land–sea temperature contrast) is at least 3 °C. The first and second filters indicate a sudden change in wind direction from offshore during the

**Table 1** Station information

| Station | Latitude (°N) | Longitude (°E) | Variable <sup>a</sup>   | Height (m MSL) | Distance from coastline (km) |
|---------|---------------|----------------|---|----------------|------------------------------|
| PCD-S   | 12.735        | 101.136        | TEMP <sub>2</sub>   | 49             | 8.0                          |
| PCD-T   | 12.730        | 101.143        | TEMP <sub>2</sub> , WS <sub>50, 100</sub> , and WD <sub>50, 100</sub> | 41             | 6.3                          |
| DEDE-T  | 12.678        | 101.063        | WS <sub>30, 40</sub> and WD <sub>40</sub>                             | 15             | 0.4                          |

TEMP Temperature, WS wind speed, WD wind direction

<sup>a</sup> Each subscript denotes the measurement height (m AGL)



nighttime to onshore during the daytime, while the third presents the degree of the thermally driven force for SB formation. In Furberg et al. (2002), there is a difference in the third filter, where daily averaged temperature (between sunrise and sunset) is used and the contrast is set to be larger than 0 °C instead. In this study, those by Borne et al. and associated results were mainly used and discussed, while results based on Furberg et al. were supplementary for comparison. SST data in the study are daily 0.5°-resolution real time global (RTG) SST data from the National Centers for Environmental Prediction (NCEP) (USA) (Gemmill et al. 2007), and, when used in the third filter, they are the spatial average of SST values in the rectangular area next to the Rayong coast (Fig. 1b). Local sunrise and sunset times were obtained from routine public reporting of TMD.

#### 2.4 Meteorological modeling

Mesoscale meteorological modeling was employed to complement the SB characterization, especially for aspects which the observed data may not be able to show or explicitly reveal (e.g., vertical profile, circulation, SB horizontal and vertical extents, and interaction with background winds). The MM5 model (version 3.7) (Grell et al. 1994), which is publicly available, was adopted for use. Four two-way interactive nested domains (D1–D4) were set up for simulations, with the horizontal resolutions of 54, 18, 6, and 2 km, respectively (Fig. 1a). As seen, the coverage of the finest-resolution domain (D4) was designed to be large enough to aid investigation of the potential interaction between SBs from both the Rayong coast (east–west aligned) and Chonburi coast (north–south aligned), and also to support the case of deep SB inland penetration. Each domain has 35 vertical sigma layers, with 18 layers within 1.5-km AGL and the thickness of the lowest layer being over 9 m, and a top pressure of 100 hPa. The key physics options used in the modeling are Kain-Fristch 2 (Kain 2004) cumulus parameterization, ETA (Mellor-Yamada) planetary boundary layer (PBL) scheme (Janjic 1994), Noah land surface model (LSM) (Chen and Dudhia 2001), and shallow cloud option. This combination of options was used based on results from a number of preliminary sensitivity experiments performed at the beginning of the study (details not shown here), and it was found to give a fair-to-acceptable prediction performance on both near-surface wind and temperature (see Sect. 3.2). It is commonly acknowledged that modeled results are sensitive to physics choices, importantly PBL and LSM parameterizations (Miao et al. 2008 and references therein). In Miao et al. (2007), a combination of the ETA PBL scheme and the Noah LSM was shown to perform reasonably over a coastal urban/built-up area with other mixed land covers in

Sweden. Six-hourly 1°-resolution NCEP FNL reanalysis data (NCEP 2010) and the daily RTG SST data were used to specify the model's initial and lateral boundary conditions. Gridded four-dimensional data assimilation (FDDA) with FNL reanalysis data was also applied to D1, and the cumulus scheme was not utilized in D3 and D4 simulations.

For land-related data required as input to the model, default model data were used, with the exception of land cover and vegetation fraction. In the study, gridded land cover data were prepared from (1) a recently released (as of the years 2006–2007) high-resolution (<200 m) Thailand land use/land cover database of the Land Development Department, Ministry of Agriculture and Cooperatives (LDD 2007) and (2) the 1-km resolution harmonized version Global Land Cover 2000 database (European Commission, Joint Research Center 2003) for areas outside Thailand. Vegetation fraction was calculated using an algorithm suggested by Gutman and Ignatov (1997) together with SPOT-VEGETATION satellite-derived monthly 1-km resolution normalized difference vegetation index (NDVI) data from the year 2006 (VITO 2010). Developed monthly vegetation fraction maps were visually examined by comparison with recent-year Landsat visible images (NASA Landsat Program 2010), and showed good agreement in spatial patterns. The intention of preparing the new land cover and vegetation fraction maps is to reflect more recent and realistic conditions of land for modeling than those given in model default (which are from the early 1990s). Figure 1c, d illustrates the developed gridded maps of both variables over D4. Table 2 compares the default

**Table 2** Percentages of land-cover categories in D4

| Category | Vegetation description         | Model default (%) | Modified (%) |
|----------|--------------------------------|-------------------|--------------|
| 1        | Urban and built-up land        | <0.1              | 4.7          |
| 2        | Dryland cropland and pasture   | 0.6               | 8.9          |
| 3        | Irrigated cropland and pasture | 19.9              | 1.1          |
| 5        | Cropland/grassland mosaic      | 0.0               | 0.4          |
| 6        | Cropland/woodland mosaic       | 3.1               | 1.8          |
| 7        | Grassland                      | <0.1              | <0.1         |
| 8        | Shrubland                      | 2.7               | 0.5          |
| 9        | Mixed shrubland/grassland      | 0.0               | 0.9          |
| 10       | Savanna                        | 0.1               | 0.0          |
| 11       | Deciduous broadleaf forest     | 1.0               | 2.3          |
| 13       | Evergreen broadleaf forest     | 6.5               | 12.6         |
| 15       | Mixed forest                   | 0.1               | 0.0          |
| 17       | Herbaceous wetland             | 0.0               | 0.6          |
| 18       | Wooded wetland                 | 0.0               | 0.1          |
| 19       | Barren sparse vegetated        | 0.0               | 0.2          |

*Remark* The remaining portion is water

model data and new data over D4. From the table, large changes (in terms of total occupied area) in several land-cover categories are seen, e.g., urban and built-up (<0.1–4.7 %), dryland cropland and pasture (0.6–8.9 %), irrigated cropland and pasture (19.9–1.1 %), and evergreen broadleaf forest (6.5–12.6 %).

Two episodic days with SBs are representatively considered for simulations here, and they are 13 January and 16 March 2006. The reason for choosing these 2 days is that each is an SBD (from the SBD identification) with different background wind conditions. The former day falls in the winter and its associated background winds are generally weak under the mild influence of the northeasterly monsoon. The latter day is in the summer (i.e., the transitional period from the northeasterly to southwesterly monsoons), and its background winds appear to vary greatly with time and play a crucial role in enhancing and deterring SBs. It is noted that SBDs are minimally or not found during the wet months over the Rayong coast, due primarily to small land–sea temperature contrasts and persistent onshore background winds under the direct influence of the southwesterly monsoon during these months (see Sect. 3.1). For each episodic day, the model was run for 24 h (01–24 local time or LT, LT = UTC + 7) plus 12 h on its previous day as a model spin-up period. Simulated hourly 10-m wind speed and 2-m air temperature in each episode were compared to observations using two metrics: mean bias (MB) and root mean square error (RMSE). They are defined by

$$\text{MB} = \frac{1}{N} \sum_{i=1}^N (P_i - O_i), \text{ and} \quad (1)$$

$$\text{RMSE} = \sqrt{\frac{\sum_{i=1}^N (P_i - O_i)^2}{N}}, \quad (2)$$

where  $O_i$  is the observation at hour  $i$ ,  $P_i$  is the prediction at hour  $i$ , and  $N$  is the total number of hours considered in comparison.

### 3 Results and discussion

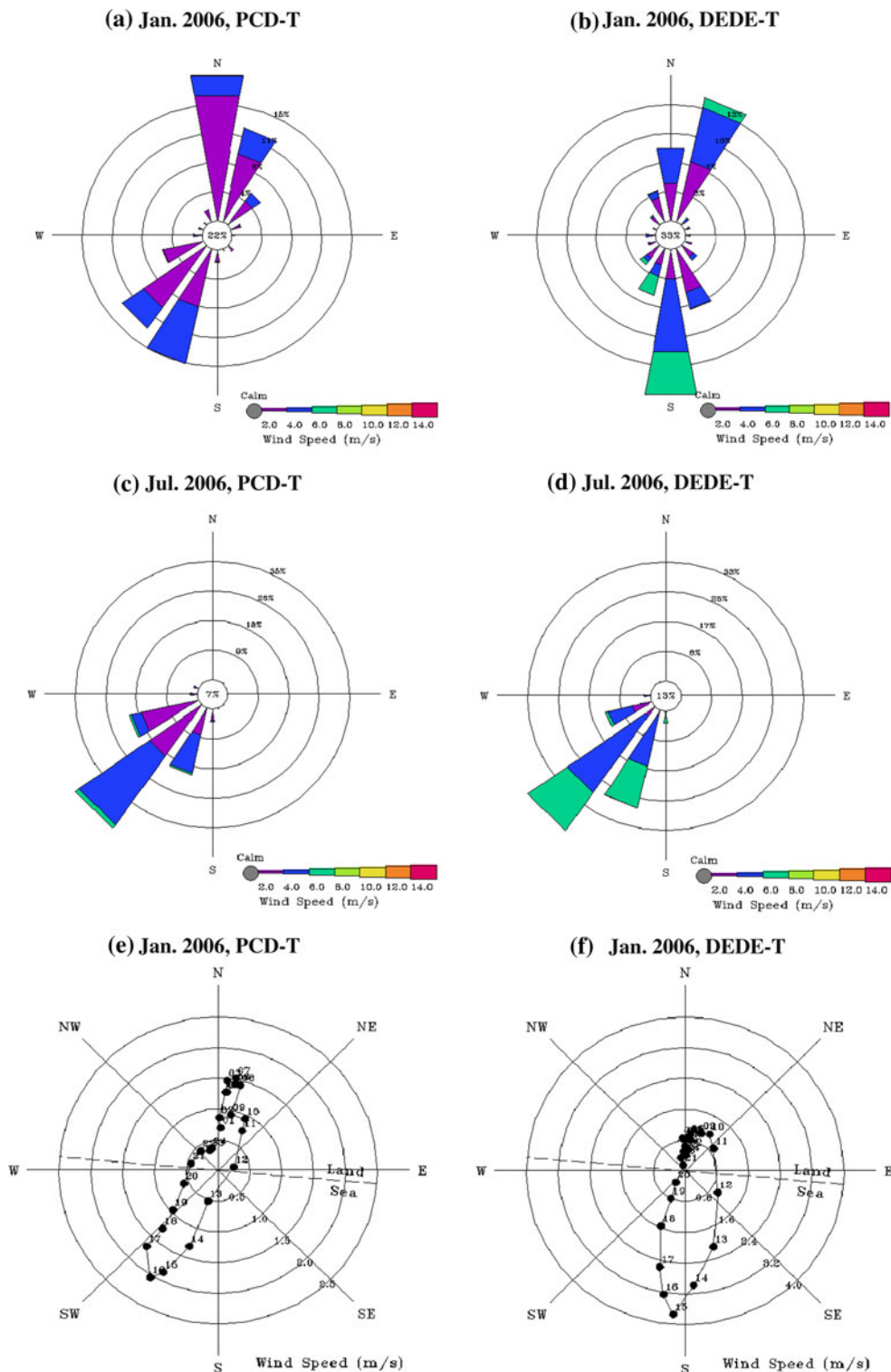
#### 3.1 Observed wind and SB characteristics

The monthly 10-m wind roses for January and July (representative of the winter and the wet season, respectively) at PCD-T and DEDE-T are shown in Fig. 2a–d (see those of all 12 months in Figs. S1 and S2 in Supplementary Materials). The wind roses at both towers are similar in pattern, and the directions of the prevailing synoptic winds (i.e., monsoons) (see Sect. 2.1) are well captured by observations. The presence of winds between the northerly

and northeasterly directions (12–70 % of hours for both towers) during October–February (i.e., winter) is consistent with the prevailing synoptic winds in these months. Southerly and southwesterly winds appear to exist (29–85 % of hours for both towers) in every month (except for November and December), which is attributable potentially to the southwesterly monsoon during May–October, to SB occurrences in January–February (Fig. 3a, b), and to the combination of SBs and background winds influenced by the synoptic conditions of the transitional monsoonal period during March–April. Based on the SBD identification using Borne et al. (1998)’s criteria, the SB develops frequently in the winter (November–February) (most often in January with 21 SBDs at PCD-T and 30 SBDs at DEDE-T). It occurs less frequently in the summer (1–4 SBDs for both towers) and minimally in the wet season ( $\leq 1$  SBD for both towers) due to decreased land–sea temperature contrasts (Fig. 4) and dominant southerly/southwesterly background winds (i.e., onshore) in the wet season, which effectively suppress SB introduction (as mentioned in Sect. 1). Maximum land–sea temperature contrasts (monthly average) are relatively large in the winter (largest in January, 4.4 °C) and become small in the wet season (smallest in June, 1.0 °C). In Fig. S3, the results based on Furberg et al. (2002)’s criteria are given for comparison. Both Borne et al.’s and Furberg et al.’s criteria show agreement that SBDs are more present in the winter. In the wet months (May–October), the latter however yields as many as 13 SBDs at PCD-T (as opposed to only 1 day as given by the former).

The monthly average (or mean) 10-m wind hodographs for January (each represents the average over all SBDs present in an individual month) at both towers are displayed in Fig. 2e, f (see those of the 12 months in Figs. S4 and S5). The corresponding mean SB onset and cessation times are also plotted in Fig. 3c, d. It is seen from the figures that winds on average turn clockwise at both towers (prominently during SB duration), which agrees with the typical rotational direction in the Northern Hemisphere (e.g., Haurwitz 1947; Simpson 1994; Furberg et al. 2002). Counterclockwise rotation may be observed in certain individual days, e.g., in the hodographs for April and August at PCD-T where only one SBD is present in each. Two potential causes for such counterclockwise rotations are (1) near-coast topography (Kusuda and Alpert 1983; Simpson 1994; Furberg et al. 2002) and (2) influence from background winds or underlying synoptic winds (Helmis et al. 1995). In the current case, it is more likely to be the latter, since the terrain of the Rayong coastal area is not too irregular or complex. The important basic SB characteristics observed in November–April are as follows. The SB begins to develop at both towers in the late morning or early afternoon. The range of mean SB onset time is 12–15

**Fig. 2** a–d Monthly 10-m wind roses (averaged over all days in month) at PCD-T and DEDE-T for January and July 2006, e–f Monthly 10-m wind hodographs (averaged over all SBDs in month) at PCD-T and DEDE-T for January 2006. In each wind rose, the number in the center denotes frequency of calms (%), and those aligned radially denote occurrence frequencies (%). In each hodograph, the number next to each solid dot denotes local time, and those aligned radially denote wind speeds (m/s)



LT at PCD-T (6–9 h after sunrise) and 1–2 h earlier at DEDE-T. A possible explanation of SBs starting several hours after sunrise is increased SB blocking due to opposing winds under the influence of the prevailing northeast monsoon during the winter. The delay at PCD-T is because it takes longer for the SB to travel to its further

inland location. Mean SB cessation time is not much different at both towers (around 18–21 LT, which is generally 1–3 h after sunset). From the hodographs, the strength of SBs at PCD-T peaks at around 15–16 LT with speeds of 2–3 m/s, while that at DEDE-T peaks 1–2 h earlier with speeds of 3–4 m/s. As seen from both towers, the SB

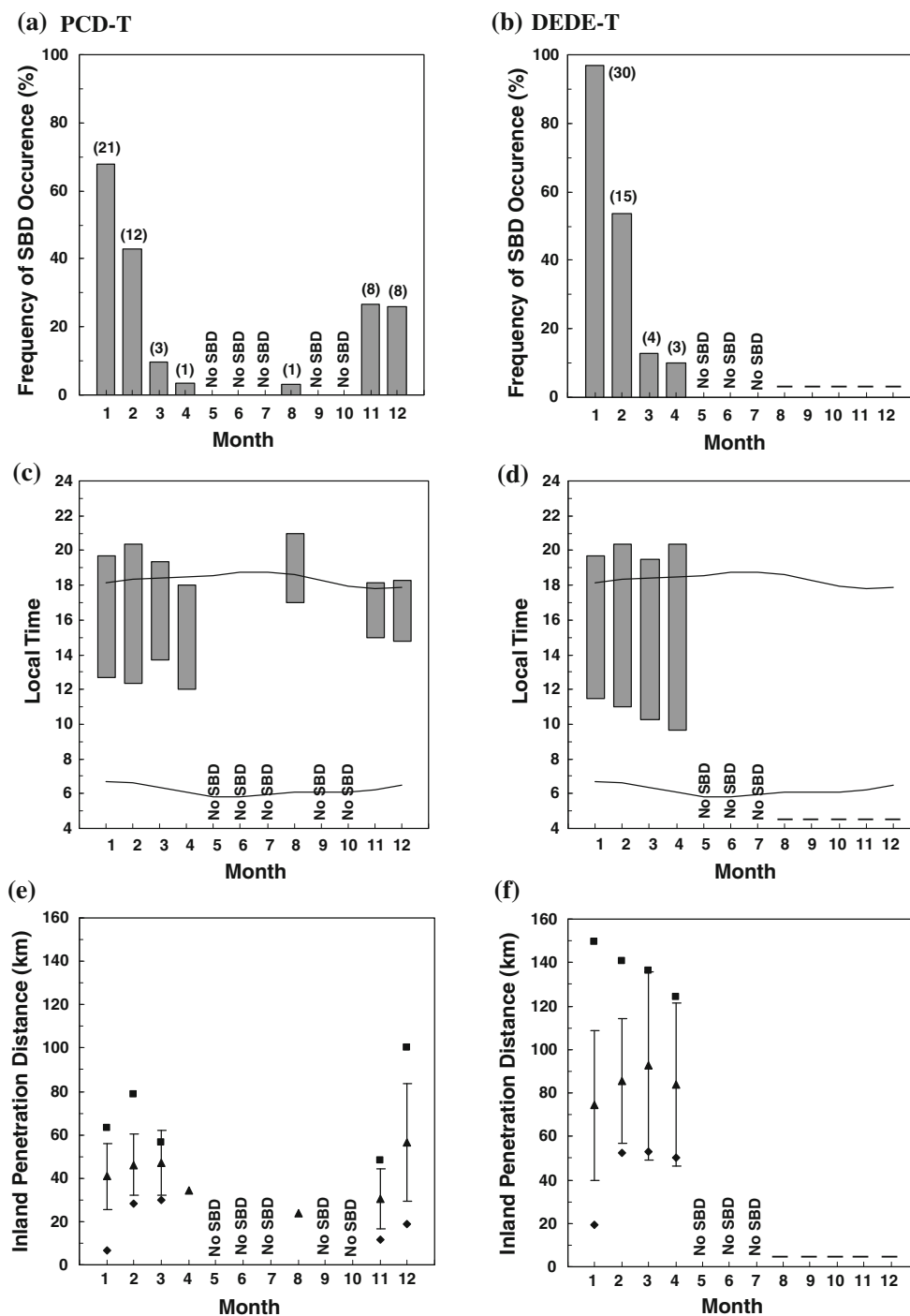


**Fig. 3** Monthly statistics of frequency of SBD occurrence, SB onset and cessation times, and inland penetration at PCD-T (**a**, **c**, **e**) and DEDE-T (**b**, **d**, **f**). In **c** and **d**, the *bottom edge*, *top edge*, and the length of each *rectangular bar* mark onset time, cessation time, and SB duration, respectively, and monthly mean sunrise and sunset times

generally peaks some time after the onset (e.g., about 1–4 h in the winter months).

In the nighttime, land breeze develops, and its strength is generally weaker than its counterpart. Mean

are shown by the *solid lines*. In **e** and **f**, each *bar* shows mean  $\pm$  standard deviation, and symbols (*filled squares* and *filled diamonds*) mark maximum and minimum, respectively. The symbol (*minus*) denotes “unavailable due to missing data”

SB duration varies greatly (3–8 h at PCD-T and 8–11 h at DEDE-T). Although the winter months from November to January are under the similar strong influence of the northeasterly monsoon, the duration appears to be



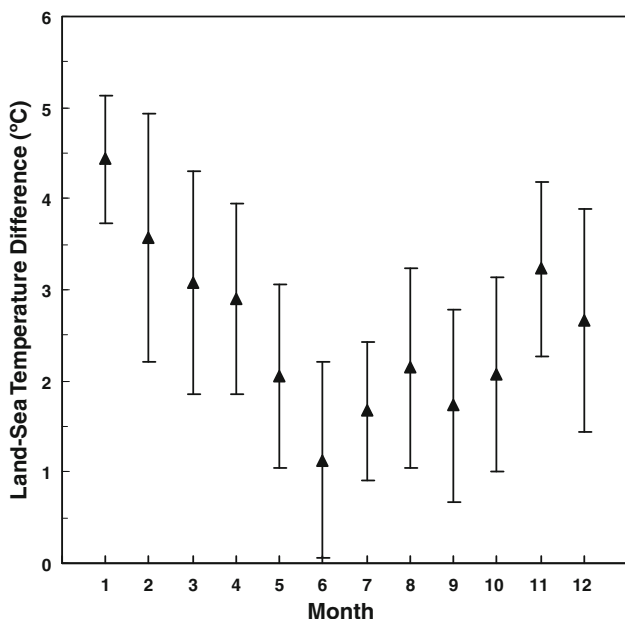


Fig. 4 Monthly land-sea temperature difference. Each bar shows mean  $\pm$  standard deviation

relatively short during November–December, which is likely due to the smaller degree of thermal forcing caused by decreased land–sea temperature contrasts. It should be noted that the mean SB duration derived from SBDs by Furberg et al.’s criteria appears to be longer with earlier SB onset and later SB cessation, compared to that by Borne et al.’s (Fig. S3).

The monthly statistics of SB inland penetration at both towers are given in Fig. 3e, f. The distance of inland penetration on an SBD was estimated based on tracking an assumed air parcel that starts from a monitoring site at the onset time and travels horizontally inland over the entire duration of the SB with hourly speed and direction values observed at that particular site, and the farthest distance (perpendicular to the coast) during the air parcel’s migration was recorded as the inland penetration distance on that SBD. This assumption is somewhat crude, as it ignores the inhomogeneity of the wind field, decrease in wind speeds due to surface friction, and the air parcel’s vertical motion. Accordingly, when a homogeneous wind field is present, the inland penetration given by the above procedure is expected to be overestimated. This technique was used here to estimate the statistics of potential inland penetration in support of a study area without a dense network of wind monitoring sites and also to approximate the horizontal extent of a simulation domain for SB modeling. Mean inland penetration (monthly averages over all SBDs) found here is 25–55 km at PCD-T and are larger (75–90 km) at DEDE-T (due mainly to smaller wind speed values observed at the further inland PCD-T, as mentioned above).

### 3.2 Simulated results on 13 January 2006

The hourly variations of both observed and simulated 10-m winds at both towers show acceptable agreement (Fig. 5a), although wind speeds tend to be overestimated (particularly, before SB onset). Considering the time interval of

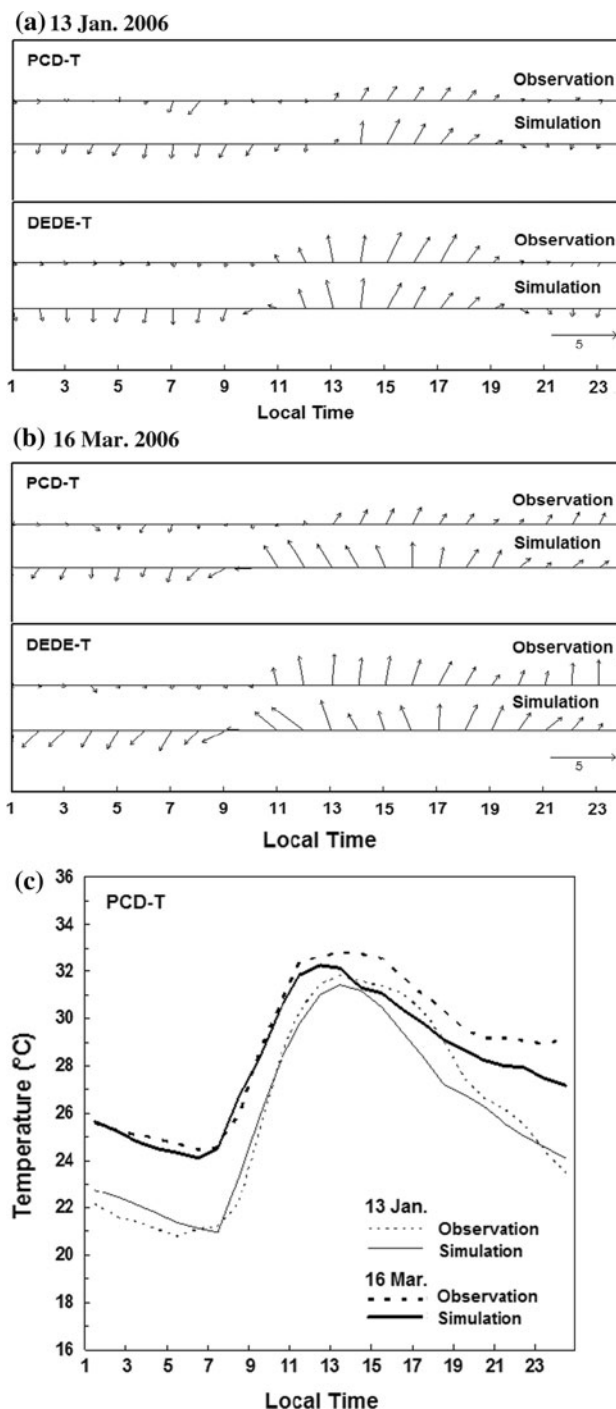


Fig. 5 Comparison between observed data and simulated results: a, b 10-m winds and c 2-m temperature. Wind vectors are in units of m/s

10–21 LT (i.e., from 1 h before SB onset to 1 h after SB cessation), MB (on wind speed) was  $<0.1$  m/s at DEDE-T and 0.5 m/s at PCD-T, and RMSE = 0.7 m/s at both stations. For 2-m temperature, the model performs fairly and give underestimates in the afternoon. Over the same time interval, MB =  $-0.9$  °C and RMSE = 1.1 °C at PCD-T (Fig. 5c). At PCT-T, the daily maximum temperature is at 13 LT in both the simulation (31 °C) and observations (32 °C). The onset and cessation times are well predicted by the model. Due to its location closer to the sea, DEDE-T encounters the SB at 11 LT, around 2 h earlier than PCD-T (13 LT), which is seen from winds switching direction from offshore to onshore. The SB cessation time is around 20 LT at both towers.

On this SBD, the background winds over East Thailand and its adjacent sea (i.e., the upper Gulf of Thailand) are concisely described as follows: Based on examination of the FNL data, upper-air (850 mb) winds tend to be northeasterly and northerly (which is under the direct influence of the northeasterly monsoon) without a drastic change in wind field pattern, while near-surface (10 m) winds instead change dynamically over time. The evolution of the SB is displayed by a series of simulated D4 wind fields over time (here at 07, 11, 15, 17, and 19 LT) (Fig. 6a–e). At 07 LT, winds over the Rayong coastal area are still offshore (i.e., land breeze), relatively weak over land (1–4 m/s), and stronger over water (3–7 m/s) due to lower surface friction. Air temperature over land increases quickly in the subsequent hours from 21 °C (07LT) to 29 °C (11 LT) at PCD-T (Fig. 5c) due to increased sensible heat from the ground heated by solar radiation. At 11 LT, wind direction begins to rotate onshore. In subsequent hours, SB becomes more mature and penetrates deep inland. Notice that SB also develops along the Chonburi coast. At 15 LT, there exist two SB fronts (one along each coast), as marked with thick gray lines in Fig. 6c. The front along the Rayong coast is around 10–15 km inland with a maximum speed of around 4 m/s, while the front along the Chonburi coast is not as deep. Both fronts meet in the southwest corner of the eastern region (shortly, the southwest land corner), and at 17 LT, continued inland penetration by both fronts leads to a merged front with a large area coverage by the SB. The convex curvature of the Rayong coast area appears to potentially enhance winds in the middle of the coast (as seen in Fig. 6c)—winds over water off the southwest land corner flow and then converge with those off the Rayong coast. Toward the evening, the SB and its strength slowly diminish and then cease.

The representative cross sections of simulated potential temperature and SB circulation, divergence, and vertical winds at 101.15°E (lon.) and 12.2°–13.3°N (lat.) at 15 LT on 13 January are displayed in Fig. 7a–c, respectively. The position of the cross-sectional plane considered is shown in Fig. 6c, passing directly through the middle of the study

area. At this hour, the SB is maturely developed. The SB circulation cell shows onshore flows (SB) in the low levels and returning offshore flows (anti-SB) in the upper levels. The SB prevails up to a height of around 600 m (above the mean sea level or MSL), and the top of the cell extends up to 1,500-m MSL. The frontal passage of the SB is seen as the advancing edge of vertically aligned isothermals interfacing the cooler sea air mass and the warmer land air mass. The front is associated with ascending winds along the leading edge and return flows aloft, and with convergence (or negative divergence) (up to  $-120 \times 10^{-5}$  1/s) in the low levels and divergence (up to  $100 \times 10^{-5}$  1/s) in the upper levels. SB-associated updraft speed at the front is relatively strong (0.1–0.5 m/s) when compared with the rest of the cross-sectional area. Also shown in the cross section, another convective cell is at around 20-km north of the front, but with a weaker updraft. The vertical profiles of potential temperature on this day at the location of PCD-T show an increase in thermal instability in the lower levels (within 200–300 m AGL) from the morning to the mid-afternoon (with the vertical gradient decreasing with time) and a return to less unstable and stable conditions in the evening (Fig. 7d). However, in the upper levels (e.g., 500–1,000 m AGL), no drastic change is noticed in the vertical gradient over time, as expected by a shallow convective circulation of a typical SB. A thick stable inversion layer exists aloft (from 1,200-m AGL upward), persistently over all hours. Moreover, a smaller (i.e., less thick) inversion layer is present in the lower levels, marking the top of a TIBL, which usually develops along with the SB and extends from the coast to the front. The TIBL's vertical extent can be readily indicated by an abrupt change of vertical temperature gradient, e.g., around 800-m AGL at the front (Fig. 7a). The PBL height over land at 15 LT is relatively limited (100–800 m AGL) over the Rayong coast due to the presence of the TIBL (Fig. 6f). It becomes large (1,000–1,600-m AGL) over most inland flat or non-hilly areas far from the coast due to the bulk PBL at this hour being convectively driven. The main simulated SB features on this SBD (discussed above) and also those on the other SBD are summarized in Table 3.

### 3.3 Simulated results on 16 March 2006

The hourly observed and simulated 10-m wind and 2-m temperature on this SBD at both towers are compared in Fig. 5b, c. It is seen that the model fairly reproduces the diurnal variation. Temperature is predicted well until 11 LT and then underestimated. Considering the time interval of 9–24 LT (i.e., from 1 h before SB onset until the end of day), MB and RMSE on temperature at PCD-T are  $-1.0$  and 1.1 °C, respectively. The model predicts the SB onset time earlier (than the observed time) by 2 h at PCD-T and

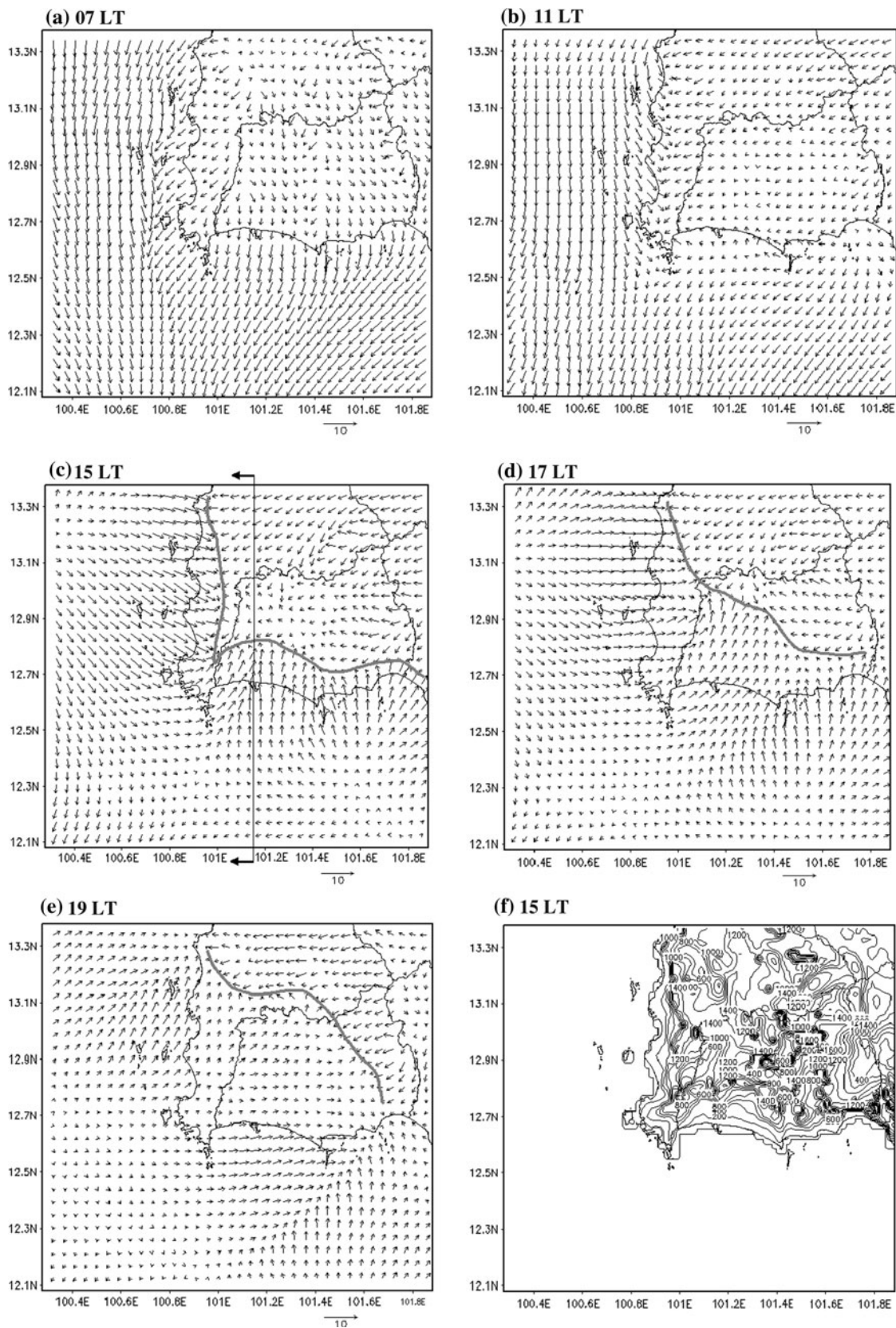


**Fig. 6** a–e Simulated 10-m winds on 13 January 2006 at 07, 11, 15, 17, and 19 LT, respectively, and f simulated boundary layer heights (m AGL) over D4 at 15 LT. SB fronts are marked with thick gray lines. Wind vectors are in units of m/s

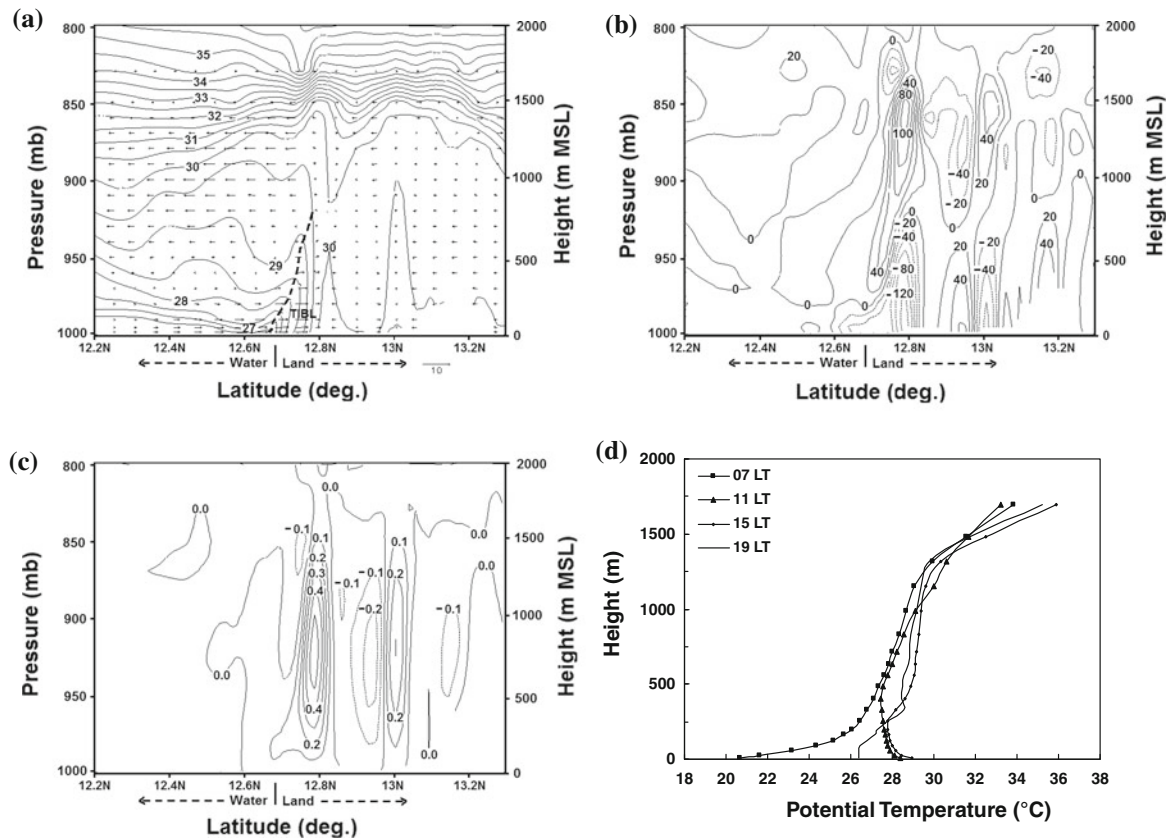


**Fig. 7** **a** Vertical cross sections (at 15 LT on 13 January 2006) of potential temperature ( $^{\circ}\text{C}$ ) and winds, **b** divergence ( $10^{-5}$  1/s), **c** vertical wind (m/s), and **d** vertical profiles of potential temperature ( $^{\circ}\text{C}$ ) at PCD-T at 07, 11, 15, and 19 LT. Wind vectors are in units of m/s

**Table 3** Simulated SB characteristics (in D4)

| Parameter   | 13 Jan. 2006         | 16 Mar. 2006                    |
|---|----------------------|---------------------------------|
| SB onset (LT) <sup>a</sup>                          | 13 (13) <sup>d</sup> | 11 (12) <sup>d</sup>            |
| SB cessation (LT) <sup>a</sup>                      | 20 (20) <sup>d</sup> | 24 or after (same) <sup>d</sup> |
| Maximum SB strength (m/s) <sup>a</sup> at 15 LT     | 4                    | 3                               |
| SB inland penetration (km) <sup>b</sup> at 15 LT    | 15                   | 45                              |
| SB vertical extent (m, MSL) <sup>c</sup> at 15 LT   | 600                  | Not seen                        |
| SB circulation cell top (m) <sup>c</sup> at 15 LT   | 1,500                | Not seen                        |
| TIBL vertical extent (m, MSL) <sup>c</sup> at 15 LT | Up to 800            | Up to 1,000                     |

<sup>a</sup> At PCD-T's location

<sup>b</sup> Distance perpendicular to the Rayong coast

<sup>c</sup> From the cross sections shown in Figs. 7, 9

<sup>d</sup> The parenthesized numbers are observed values (given here for comparison)

by 1 h at DEDE. Like 13 January, the model tends to overestimate wind speed in pre-onset hours, and the corresponding MB and RMSE at DEDE-T are 0.2 and 1.6 m/s, respectively, and at PCD-T are 1.2 and 1.7 m/s, respectively, over the same interval.

The background winds on this SBD over East Thailand, based on examination of the FNL data, are quite different from those on 13 January in many aspects. During a typical

transitional period of the two monsoons in the summer, a weak or mild high-pressure system is usually present over East Asia and drives winds downward to the tropics and the Intertropical Convergence Zone (ITCZ). They move along the South China Sea and can be enhanced by easterly winds from the Pacific Ocean. Also based on the FNL data, easterly 850-mb winds across East Thailand and the Gulf of Thailand prevails on this day. Near-surface winds vary



greatly with time. During the mid-afternoon and the evening, those over the lower-to-middle Gulf appear to turn to the north to northeast. The evolution of SB on this day is described by a series of simulated D4 wind fields over time (at 07, 11, 15, 17, and 19 LT) (Fig. 8a–e). At 07 LT, weak land breeze (1–2 m/s) is present along each of the Rayong and Chonburi coasts. At PCD-T, temperature increases rapidly from 24 °C (07 LT) to 32 °C (11 LT) (Fig. 5c). At 11 LT (as the onset time), the background winds become southeasterly and onshore over the Rayong coast and so strong that they penetrate and cross over to the Chonburi coast, as a combined result of thermally driven winds and the southeasterly/easterly background winds. At this hour, the background winds off the Chonburi coast tend to be northerly and northeasterly, and start to turn toward the coast but still are somewhat subdued in proceeding further due to opposing easterly winds. In the early afternoon along both coasts, SB gains strength due to sustained thermal contrast and the fronts are evidently seen. At 15 LT, the background winds are southerly and enhance the SB along the Rayong coast, resulting in inland penetration of up to 45 km, while inland penetration along the other coast is limited to 20 km or less. Background winds off the Chonburi coast have now changed direction to the north. SB is also observed along this coast and is relatively strong (6–7 m/s) over the middle part of the coast. In the lower part of Chonburi, the SBs from both coasts meet (as marked by the dashed line in Fig. 8c), and their fronts later merge into one. At 17 LT, both SBs become weaker due to decreased thermal forcing, whereas the background winds still prominently exist. The front along the Rayong coast recedes, while only a small frontal portion is left along the other coast. At 19 LT, only the SB along the Rayong coast still persists with reduced speed (1–4 m/s), and it is difficult to distinguish it from the southerly background winds. In subsequent hours, its strength gradually becomes smaller.

Also, notice that a divergence zone is present at about 40–50 km off the Rayong coast (12.2°N, 101.2°E) at 11 LT (Fig. 8b). Based on our examination of horizontal fields in domains D3 and D4 and associated vertical cross sections in time sequence (details not shown), this zone is somewhat transient—forming at 10–11 LT, then expanding to the northwest, and finally dissipating at 13 LT as southeasterly winds off the corner of the eastern region. This divergence zone is likely not to be a result from an SB circulation since this divergence is quite deep (i.e., not shallow), extending upward beyond the extent of the atmospheric boundary layer. The cause of its formation is not clear, but we attribute its formation to interaction of surface and background winds near the surface and aloft. At 15 LT, another but weak divergence zone is observed over the corner of the domain (12.2°N, 100.4°E) (Fig. 8c). Note that the

western border of the domain is parallel to and not far (30–40 km) from the southern coast. The time sequence examination found that winds over that corner were northerly or northeasterly until 13 LT, but later turned onshore due likely to increased thermal contrast between land and water. Nevertheless, no return flow is observed aloft (at least up to 800 hPa level) possibly because it is dominated by winds aloft (which is onshore and strong).

The cross sections of the same set of variables, previously shown in the former case, are also displayed for 15 LT on the current SBD (Fig. 9a–c). At this hour, the onshore background winds are prominent so that the SB circulation cannot be fully defined. Specifically, there is no return flow aloft seen. The convergence at or near the front extends up to 1,800-m MSL, with a maximum magnitude of  $120 \times 10^{-5}$  1/s. The front at this hour of this SBD appears to be weaker than that of the former day in terms of vertical speed in the lower levels of the front. Also, another circulation cell is seen next to the front (to the north) with a near-surface divergence of  $140 \times 10^{-5}$ /s, a maximum updraft speed of 0.6 m/s, and a maximum downdraft speed of 1.0 m/s. The vertical extent of the TIBL induced by the SB increases sharply near the coast and then gradually toward the front (up to 1,000-m MSL). Examination of the boundary layer height over land also shows relatively small values (mostly 200–600 m AGL) near the Rayong coast and large values (800–1,400 m AGL) toward the front (Fig. 8f). The boundary layer height over most of the other inland areas turns out not to be as large (200–400 m AGL), including a wide area of near-surface divergence located near the upper right corner of the domain. At the location of PCD-T, the thermal instability near the ground and the low levels increases from the morning to mid-afternoon, and becomes neutral in the evening (Fig. 9d). At 07 LT, the entire boundary layer is stable and later at 11 LT (onset time) becomes near neutral (except for heights near the surface) with a thick inversion layer seen from 1,000-m AGL upward. However, in later hours, the TIBL induced by the SB limits the height to 500-m AGL.

At the end of our discussion, it is worth mentioning that biases in meteorological modeling can come from different sources such as (1) imperfect representation of physical processes (i.e., physics parameterizations) in a model, (2) inaccuracy or uncertainty in model input, and (3) numerical errors due to space and time discretization. Miao et al. (2009) found wind speed and temperature being sensitive to choices of model physics options. In our preliminary tests performed to guide the used physics options for our simulations here, biases in both variables were observed to varying degrees with different physics option combinations. Specified values of parameters in a physics parameterization could also be a source of error. For example, Papanastasiou et al. (2010) attributed wind speed



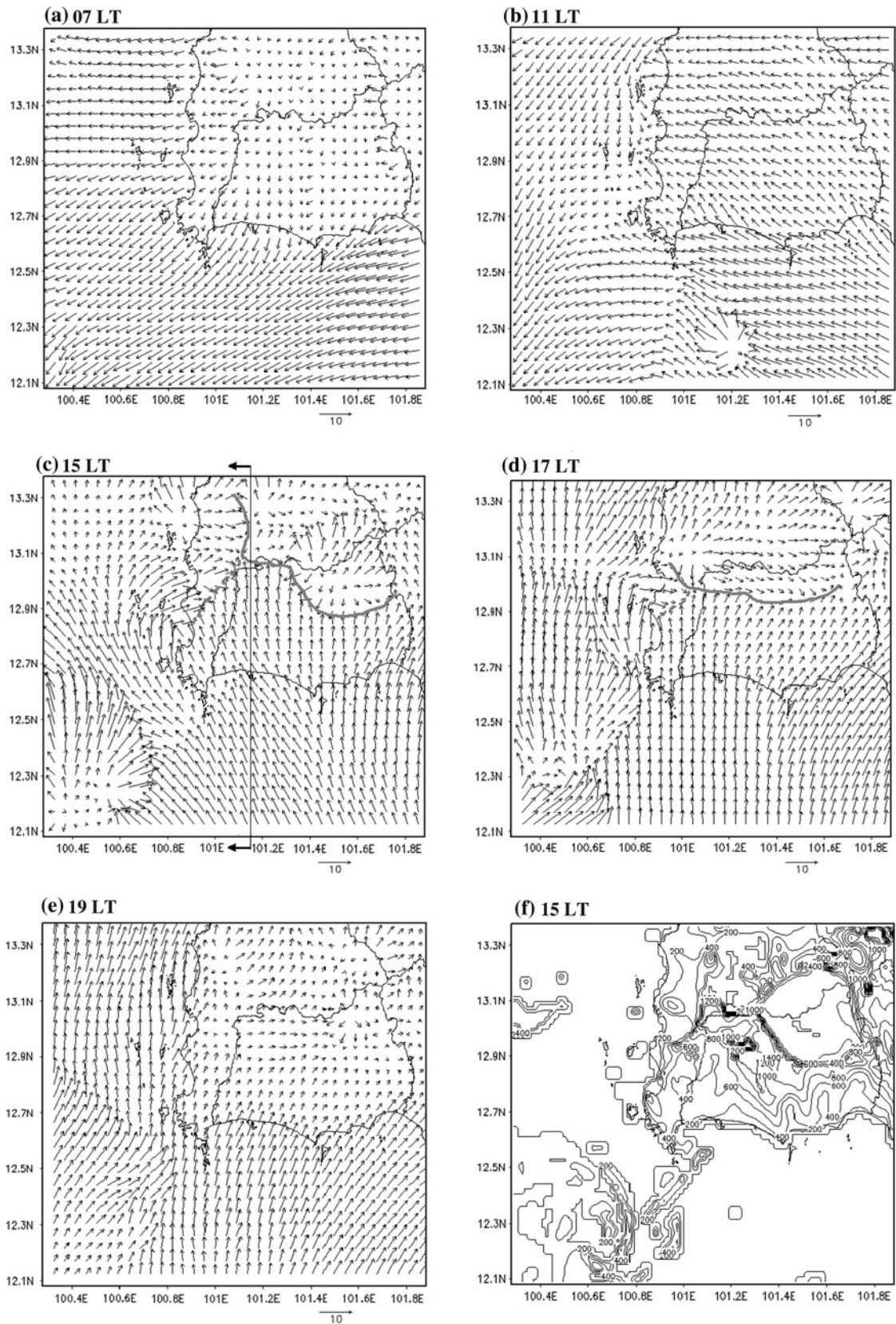


**Fig. 8** a–e Simulated 10-m winds on 16 March 2006 at 07, 11, 15, 17, and 19 LT, respectively, and f simulated boundary layer heights (m AGL) over D4 at 15 LT. SB fronts are marked with *thick gray lines*. Wind vectors are in units of m/s

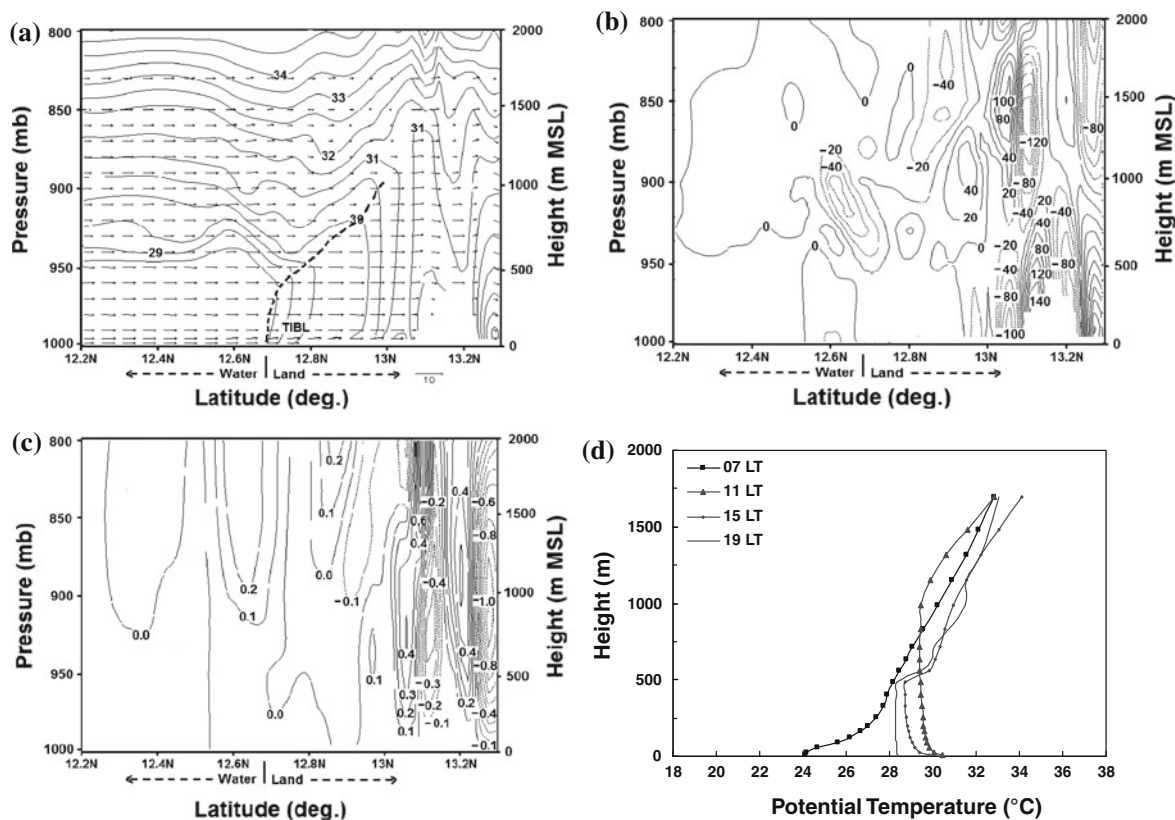


**Fig. 9** **a** Vertical cross sections (at 15 LT on 16 March 2006) of potential temperature (°C) and winds, **b** divergence ( $10^{-5}$  1/s), **c** vertical wind (m/s), and **d** vertical profiles of potential temperature (°C) at PCD-T at 07, 11, 15, and 19 LT. Wind vectors are in units of m/s

overpredicted by the WRF model in their SB study over an urban area in central Greece to low surface roughness length ( $z_0$ ) for urban area in the model, which could potentially be our case here ( $z_0$  for urban in MM5 being set to 0.5; since large industrial facilities and power plants exist in the study area). As for our temperature underestimation, its degree tends to become larger in the afternoon—in line with the results of Papanastasiou et al. (2010) where a need to appropriately account for urban energy balance in their applied model was reflected.

#### 4 Conclusions

The SB and its associated boundary layer structure over the Rayong coastal area in the eastern region of Thailand were studied using both observation data analysis and fine-resolution (2 km) mesoscale modeling with the MM5 model. The land cover and satellite-derived vegetation fraction data utilized in the modeling were specifically prepared to reflect more realistic land conditions for the study area. The availability of high-quality wind data from the two monitoring towers for the year 2006 allowed basic SB characterization to be possible, and the numerical simulations

helped reveal or identify additional SB features. The key SB characteristics and important findings obtained from the study are given below:

1. Over the Rayong coast, SB occurs most frequently in the winter months due mainly to relatively large land–sea temperature contrasts. The decreased temperature contrasts and the onshore background winds under the strong influence of the southwesterly monsoon are considered the main factors of the minimal SB presence in the wet season.
2. The mean observed SB onset and cessation times are at around 12–15 LT and 18–21 LT, respectively. The mean SB duration ranges from 3 to 11 h. The strength of SB peaks during the early- to mid-afternoon. In general, SB exhibits a clockwise rotation on average. The degree of inland penetration (inferred from the observed wind data at PCD-T tower) ranges widely with the monthly means of 25–55 km from the coast. These results are based on using Borne et al. (1998)'s SBD criteria. In fact, how an SBD is identified indeed depends on (i.e., is sensitive to) a specific set of SBD criteria applied. We also computed results derived from Furberg et al. (2002)'s SBD criteria and found that both produce similar results, in that SBDs are

more present in the winter. However, Furberg et al tend to yield more SBDs in wet months than Borne et al.

3. In the MM5 simulations, two SBDs, which are 13 January (winter) and 16 March (summer) in 2006, were chosen as representative for the case of weak background winds and the case of strong influence from onshore background winds, respectively. However, simulated near-surface wind and temperature are in fair-to-acceptable agreement with the observations on the two SBDs.
4. On the former SBD, the SB circulation on the Rayong coast is clearly defined with a return flow aloft and in front. Another SB on the west side of the eastern region (i.e., along the Chonburi coast) also develops separately, but their fronts merge into one in the mid-afternoon, resulting in a large area coverage by the SB. Both SBs cease in the early evening. On the latter SBD, the SB over the Rayong coast is enhanced by the onshore background winds, penetrating inland deeply (e.g., 45 km in the mid-afternoon) and persisting until late evening. However, the SB along the other coast is somewhat subdued until early afternoon by the offshore background winds. On both days, the degree of inland penetration from the Rayong coast tends to be larger than the other coast. As shown, the PBL height over the area covered by an SB can be significantly affected by the presence of a TIBL, which is very low near the Rayong and Chonburi coasts and increases toward the SB front (e.g., 800–1,000 m in the mid-afternoon over the Rayong coast).

The investigation presented here shows the evident presence of SBs along the Rayong coast, Thailand. The issues of deep inland penetration and TIBL formation suggested by the results encourage further studies on a potential link of the roles of SB and local air pollutant problems known to occur occasionally, specifically in terms of the horizontal transport and vertical mixing extents of air pollutants over this highly industrialized coastal area. Moreover, since this study is limited to only 2006, an extended study in the future covering a longer-term period could be useful to understand SB climatology and interannual variability.

**Acknowledgments** The authors sincerely thank the Pollution Control Department, the Department of Energy Development and Efficiency, the Land Development Department, and the Thai Meteorological Department for providing local data, the National Center for Atmospheric Research (US) for the availability of the MM5 model, and the National Centers for Environmental Protection (US) for the FNL Reanalysis and RTG SST data. The authors also thank Dr. Robert H. B. Exell and Dr. Chumnong Sorapipatana (JGSEE), Dr. Dusadee Sukawat (KMUTT), Mr. Nawarat Mitjit (PCD), and the two anonymous reviewers for their useful comments

and suggestions. Assistance by members at the JGSEE computational laboratory is acknowledged. This study was financially supported mainly by the JGSEE and the Thailand Research Fund (under Grant No. RDG5050016) and partially by the Postgraduate Education and Research Development Office (under Grant No. JGSEE/PROJECT/002-2011) and the National Research Council of Thailand (under Grant No. POR KOR 2550-46).

## References

- Abbs DJ, Physick WL (1992) Sea breeze observations and modeling: a review. *Aust Meteorol Mag* 41:7–9
- Arritt RW (1992) Effects of the large-scale flow on characteristic features of the sea breeze. *J Appl Meteor* 32:116–125
- Azorin-Molina C, Chen D (2008) A climatological study of the influence of synoptic-scale flows on sea breeze evolution in the Bay of Alicante (Spain). *Theor Appl Climatol* 96:249–260
- Borne K, Chen D, Nunez M (1998) A method for finding sea-breeze days under stable synoptic conditions and its application to the Swedish west coast. *Int J Climatol* 18:901–914
- Cai XM, Steyn DG (2000) Modelling study of sea breezes in a complex coastal environment. *Atmos Environ* 34:2873–2885
- Chen F, Dudhia J (2001) Coupling an advanced land–surface/hydrology model with the Penn State/NCAR MM5 modeling system. Part I: model implementation and sensitivity. *Mon Wea Rev* 129:569–585
- Chen XL, Feng YR, Li JN, Lin WS, Fan SJ, Wang AY, Fong SK, Lin H (2009) Numerical simulations on the effect of sea–land breezes on atmospheric haze over the Pearl River Delta region. *Environ Model Assess* 14:351–363
- Crosman ET, Horel JD (2010) Sea and lake breezes: a review of numerical studies. *Bound Layer Meteorol* 137:1–29
- Dandou A, Tombrou M, Soulakellis N (2009) The influence of the city of Athens on the evolution of the sea breeze front. *Bound Layer Meteorol* 131:35–51
- Ding AJ, Wang T, Zhao M, Wang TJ, Li ZK (2004) Simulation of sea–land breezes and a discussion of their implications on the transport of air pollution during a multi-day ozone episode in the Pearl River Delta of China. *Atmos Environ* 38:6737–6750
- European Commission, Joint Research Centre (EC-JRC) (2003) Global Land Cover 2000 database Website: <http://bioval.jrc.ec.europa.eu/products/glc2000/glc2000.php>. Accessed: September 2009
- Furberg M, Steyn DG, Baldi M (2002) The climatology of sea breezes on Sardinia. *Int J Climatol* 22:917–932
- Gemmill, William, Bert Katz, Xu Li (2007) Daily real-time global sea surface temperature-high resolution analysis at NOAA/NCEP. NOAA/NWS/NCEP/MMAB Office Note Nr. 260. Website: <http://polar.ncep.noaa.gov/sst>. Accessed September 2008
- Grell GA, Dudhia J, Stauffer DR (1994) A Description of the fifth generation Penn State/NCAR mesoscale model (MM5). Technical Note, NCAR, Boulder, Colorado, US
- Gutman G, Ignatov A (1997) Satellite derived green vegetation fraction for the use in numerical weather prediction models. *Adv Space Res* 19:477–480
- Hadi TW, Horinouchi T, Tsuda T, Hashiguchi H, Fukao S (2002) Sea-breeze circulation over Jakarta, Indonesia: a climatology based on boundary layer radar observations. *Mon Wea Rev* 130:2153–2166
- Haurwitz B (1947) Comments on the sea-breeze circulation. *J Meteorol* 4:1–8
- Helmis CG, Papadopoulos KH, Kalogiros JA, Soilemes AT, Asimakopoulou DN (1995) Influence of background flow on evolution of Saronic Gulf sea breeze. *Atmos Environ* 29:3689–3701

- Janjic ZI (1994) The step-mountain ETA coordinate model: further development of the convection, viscous sublayer and turbulent closure schemes. *Mon Wea Rev* 122:927–945
- Joseph B, Bhatt BC, Koh TY, Chen S (2008) Sea breeze simulation over the Malay Peninsula in an intermonsoon period. *J Geophys Res* 113:d20122. doi:10.1029/2008jd010319
- Kain JS (2004) The Kain-Fritsch convective parameterization: an update. *J Appl Meteor* 43:170–181
- Kusuda M, Alpert P (1983) Anti-clockwise rotation of the wind hodograph. Part I: theoretical study. *J Atmos Sci* 40:487–499
- LDD (2007) Land use and land cover data of Thailand for the years 2006–2007. CD-ROM Product, Ministry of Agriculture and Cooperatives, Thailand
- Lin WS, Wang AY, Wu CS, Fong SK, Ku CM (2001) A case modeling of sea-land breeze in Macao and its neighborhood. *Adv Atmos Sci* 18:1231–1240
- Lu X, Chow KC, Yao T, Lau AKH, Fung JCH (2009) Effects of urbanization on the land sea breeze circulation over the Pearl River Delta region in winter. *Int J Climatol* 30:1089–1104
- Manomaiphiboon K, Prabamroong A, Chanaprasert W, Rajpreeda N, Phan TT (2010) Dual database system of wind resource for Thailand. Final Report of Project “Wind Resource Assessment Using Advanced Atmospheric Modeling and GIS Analysis”, Joint Graduate School of Energy and Environment, King Mongkut’s University of Technology Thonburi (in Thai, with English Abstract). Website: [http://complabkt.jgsee.kmutt.ac.th/wind\\_proj](http://complabkt.jgsee.kmutt.ac.th/wind_proj) Accessed: August 2010
- Miao JF, Kroon LJM, Vilà-Guerau de Arellano J, Holtslag AAM (2003) Impacts of topography and land degradation on the sea breeze over eastern Spain. *Meteorol Atmos Phys* 84:157–170
- Miao JF, Chen D, Borne K (2007) Evaluation and comparison of Noah and Pleim-Xiu land surface models in MM5 using GÖTE2001 data: spatial and temporal variations in near-surface air temperature. *J Appl Meteor Climatol* 46:1587–1605
- Miao JF, Chen D, Wyser K, Borne K, Lindgren J, Strandvall MKS, Thorsson S, Achberger C, Almkvist E (2008) Evaluation of MM5 mesoscale model at local scale for air quality applications over the Swedish west coast: influence of PBL and LSM parameterizations. *Meteorol Atmos Phys* 99:77–103
- Miao JF, Wyser K, Chen D, Ritchie H (2009) Impacts of boundary layer turbulence and land surface process parameterizations on simulated sea breeze characteristics. *Ann Geophys* 27:2303–2320
- Miller STK, Keim BD, Talbot RW, Mao H (2003) Sea breeze: structure, forecasting, and impacts. *Rev Geophys* 41:1–31
- NASA Landsat Program (2010) Landsat scenes from epoch 2005 collection. Website: <http://landsat.usgs.gov>. Accessed August 2010
- National Centers for Environmental Prediction (NCEP) (2010) FNL operational model global tropospheric analyses. Website: <http://dss.ucar.edu/datasets/ds083.2>. Accessed September 2008
- Papanastasiou DK, Melas D (2009) Climatology and impact on air quality of sea breeze in an urban coastal environment. *Int J Climatol* 29:305–315
- Papanastasiou DK, Melas D, Lissaridis I (2010) Study of wind field under sea breeze conditions; an application of WRF model. *Atmos Res* 98:102–117
- Pham TBT, Manomaiphiboon K, Vongmahadlek C (2008) Development of an inventory and temporal allocation profiles of emissions from power plants and industrial facilities in Thailand. *Sci Total Environ* 397:103–118
- Pielke RA, Cotton WR, Walko RL, Tremback CJ, Lyons WA, Grasso LD, Nicholls ME, Moran MD, Wesley DA, Lee TJ, Copeland JH (1992) A comprehensive meteorological modeling system—RAMS. *Meteorol Atmos Phys* 49:69–91
- Pollution Control Department (PCD) (2007) Thailand state of pollution in 2006. Ministry of Natural Resources and Environment. Website: [http://www.pcd.go.th/count/mgtdl.cfm?FileName=Report\\_Eng2549.pdf](http://www.pcd.go.th/count/mgtdl.cfm?FileName=Report_Eng2549.pdf). Accessed: September 2009
- Pushpadas D, Vethamony P, Sudheesh K, George S, Babu MT, Nair TMB (2010) Simulation of coastal winds along the central west coast of India using the MM5 mesoscale model. *Meteorol Atmos Phys* 109:91–106
- Simpson JE (1994) Sea breeze and local winds. Cambridge University Press, New York
- Skamarock WC, Klemp JB, Dudhia J, Gill DO, Barker DM, Wang W, Powers JG (2005) A description of the advanced research WRF Version 2. Technical Note 468 + STR, NCAR, Boulder, Colorado, US
- Srinivas CV, Venkatesan R, Somayaji KM, Singh AB (2006) A numerical study of sea breeze circulation observed at a tropical site Kalpakkam on the east coast of India, under different synoptic flow situations. *J Earth Syst Sci* 115:557–574
- Thai Meteorological Department (TMD) (2010) Climate of Thailand. Ministry of Information and Communication Technology. Website: <http://www.tmd.go.th/en/archive/surfacewind.php>. Accessed: September 2009
- Thepanondh S, Varoonphan J, Sarutichart P, Makkasap T (2010) Airborne volatile organic compounds and their potential health impact on the vicinity of petrochemical industrial complex. *Water Air Soil Pollut*. doi:10.1007/s11270-010-0406-0
- van Ulden AP, Holtslag AAM (1985) Estimation of atmospheric boundary layer parameters for diffusion applications. *J. Clim Appl Meteorol* 24:1196–1207
- VITO (2010) Free vegetation products. Flemish Institute for Technological Research, Belgium. Website: <http://free.vgt.vito.be>. Accessed September 2009